Release of helium from vacancy defects in yttria-stabilized zirconia under irradiation

Xin Ou,[1,*] Reinhard Kögler,[1] Hong-Bo Zhou,[2] Wolfgang Anwand,[1] Jörg Grenzer,[1] René Hübner,[1] Matthias Voelskow,[1] Maik Butterling,[1] Shengqiang Zhou,[1] and Wolfgang Skorupa[1]
[1]*Helmholtz-Zentrum Dresden-Rossendorf (HZDR) e.V., P.O. Box 510119, 01314 Dresden, Germany*
[2]*Department of Physics, Beihang University, Beijing 100191, China*
(Received 9 August 2012; revised manuscript received 5 November 2012; published 5 December 2012)

Fission gas retention or release has a critical impact on the function of advanced nuclear materials. Helium trapping in, and release from, radiation defects induced by neutrons and by α decay in YSZ (yttria-stabilized zirconia) is experimentally simulated using synchronized Zr^+ and He^+ dual ion beam irradiation. The measured damage profiles consist of two peaks which agree well with the calculated profiles of implantation induced excess point defects. This special implantation related effect has to be carefully considered in the evaluation of experimental investigations which simulate isotropic irradiation effects such as α decay. First-principles calculations show that helium is energetically favorable to be trapped by Zr vacancies in YSZ. Implanted helium alone in YSZ is accumulated in undesirable helium bubbles and results in local surface swelling and lift-off. However, under dual beam irradiation helium is released from vacancy defects and is out-diffused at room temperature. Helium is mobilized by a vacancy-assisted trapping/detrapping mechanism induced by the simultaneous Zr^+ ion implantation. This behavior avoids the deleterious helium bubble formation and contributes to the suitable application characteristics of YSZ which result in its excellent radiation hardness.

DOI: 10.1103/PhysRevB.86.224103 PACS number(s): 61.80.Jh, 61.82.Ms

I. INTRODUCTION

The safety of nuclear energy is a main issue worldwide. The challenges including the disposal of actinides generated in the nuclear reactors and nuclear waste management need to be overcome by intensive scientific studies.[1] Investigations of the radiation damage in nuclear materials are important to understand and to develop radiation resistant materials.[2,3] Cubic YSZ (yttria-stabilized zirconia) is fabricated by doping the zirconia with 8 mol % yttria. The cubic phase of pure zirconia only exists at temperatures above 2370 °C. Yttria stabilizes the cubic phase zirconia to room temperature. This single crystalline material is a suitable model system for the investigation of the class of materials. Due to its high radiation resistance and high chemical stability, YSZ can be applied for the intermatrix layer of nuclear fuel or for the covering and storage of nuclear waste, for instance, for actinide transmutation or immobilization.[4–6]

The irradiation effect on YSZ is the most critical concern and must be investigated with respect to neutron exposure and α decay of actinides. It was demonstrated that ion beam irradiation is a simple and very efficient tool to simulate the radiation damage in nuclear materials.[7] The radiation effect in zirconia has been intensively investigated in recent years by ion beam irradiation.[8–17] Most of the experimental works were performed using He^+ ion implantation to simulate the radiation damage induced by α particles[15–17] or by implantation of heavy ions such as $C_S{}^+$, I^+, and Xe^+ to simulate the neutron radiation damage and the damage introduced from α recoils.[6,8,10] In fact, the simultaneous dual beam implantation of heavy ions and He^+ ions is the most realistic simulation of the real radiation damage created in nuclear equipment or in the cover of nuclear waste. Such experiments give us the opportunity to study the interdependence of the radiation damage resulting from neutron radiation and from α-particle radiation. However, this case was not reported yet on YSZ in the literature.

In this work the simultaneous dual beam implantation of YSZ by Zr^+ and He^+ ions is performed. The damage induced in YSZ is investigated by a set of complementary analysis methods which are sensitive for defects on the nanometer scale and even below.

Moreover, a special difference in damage formation is highlighted between neutron irradiation and α decay on the one hand and ion implantation on the other hand. The first one is an isotropic radiation, whereas the latter is a directed one. Point defects are generated along the ion path where vacancies and interstitials are separated due to momentum transfer conservation and predominant forward scattering. Vacancies are accumulated at the depth position before the projected ion range (R_p), and interstitials are accumulated around R_p. The vacancy cluster formation approximately at the depth position around half of R_p is termed the "$\frac{1}{2}R_p$" effect and was carefully investigated and well understood in single crystalline silicon because of its important application in impurity gettering processes.[18–21] Saudé *et al.*[22] observed trapping of the helium atoms implanted with high fluence of 1×10^{17} cm^{-2} into YSZ by a self-generated $\frac{1}{2}R_p$ effect. Implanted helium tends to occupy vacancy sites in a crystalline substrate and in this way it stabilizes vacancies and vacancy clusters by pressurization, which possibly leads to a deleterious effect on the microstructure and the mechanical properties of the substrate.[22,23] Such defect behavior has to be carefully considered when the radiation induced damage in YSZ is evaluated. Dual beam irradiation (heavy ions and He^+) gives an unique and worthy opportunity to investigate the interaction of helium atoms with the vacancy defects generated by the simultaneous heavy ion irradiation. This is of importance as heavy ion irradiation generates a much larger amount of vacancy defects per helium atom as compared with helium irradiation alone, and it also induces a significant energy deposition on the YSZ lattice, which may have a great impact on the status of helium trapped inside.

 ©2012 American Physical Society

II. EXPERIMENT

(100)-oriented single crystalline YSZ samples with a size of 1×1 cm^2 were implanted at room temperature with Zr^+ and He^+ ions of 2.5 MeV and 100 keV and ion fluences of 1×10^{16} and 5×10^{15} cm^{-2}, respectively. He^+ ion energy was chosen in order to fit the helium profile with the excess vacancy profile (at $\frac{1}{2} R_p$) generated by the Zr^+ ions. He^+ ions were also complementary implanted with a higher fluence of 1×10^{16} cm^{-2} and with an energy of 260 keV in order to fit the profile with that of the Zr^+ ions. Implantations were performed at the dual ion beam facility of the Helmholtz-Zentrum Dresden-Rossendorf.[24] This equipment consists of two independent beam lines from a conventional 500 kV implanter and from a 3 MV Tandetron accelerator which are connected under an angle of 45°. The irradiation with Zr^+ and He^+ ions was performed in synchronous dual beam (DB) mode and also in single beam mode for reference. The Zr^+ implantation results in a maximum damage in ZrO_2 of 21 dpa and a helium content of 105 ppm He/dpa. Part of the samples was annealed at 800 °C for 1 h under atmosphere of 5% O_2 and 95% Ar. The ion induced damage in the YSZ crystal was determined by Rutherford backscattering spectrometry (RBS) with 1.7 MeV He^+ ions detected at a backscattering angle of 170°. The lattice strain was profiled by high resolution x-ray diffraction (HRXRD). A Seifert-GE XRD3003HR diffractometer operating at the $Cu_{K\alpha 1}$ wavelength was equipped with a spherical two-dimensional (2D) Goebel mirror allowing a beam size on the order of 1 mm horizontally and vertically. To achieve the highest angular resolution a Bartels monochromator and a triple-axis analysator were installed in front of the scintillation counter. The crystal morphology was studied by cross-sectional transmission electron microscopy (TEM) and high resolution TEM (HRTEM). Moreover, open volume defects in the samples were investigated using the positron annihilation spectroscopy (PAS). That means the monitoring of the 511 keV annihilation radiation by conventional Doppler broadening spectroscopy and by the coincidence Doppler broadening spectroscopy. The surface topography of the ZrO_2 surface was measured by atomic force microscopy (AFM).

III. RESULTS

A. TRIM Monte Carlo simulation

The depth profiles of implanted Zr and He atoms and the related damage were calculated by Monte Carlo simulation with the computer code of transport of ions in matter (TRIM).[25] Figure 1 shows depth profiles in ZrO_2 of the implanted Zr^+ and He^+ ions. The profile of the total amount of displacements of Zr and O atoms (V_{TOT}) is also shown. The damage generation (dpa) by Zr^+ ions exceeds that of He^+ ions by a factor of 130. Consequently, He-induced damage can be neglected. A full cascade TRIM simulation[25,26] allows for the calculation of excess point defects, either vacancies or interstitials. Excess vacancies and excess interstitials are point defects that remain after the complete local point defect recombination. The depth profiles of the remaining excess of vacancies V_{EX} and interstitials I_{EX} are calculated for Zr^+ implantation and are also shown in Fig. 1. These profiles represent the as-implanted state without considering any

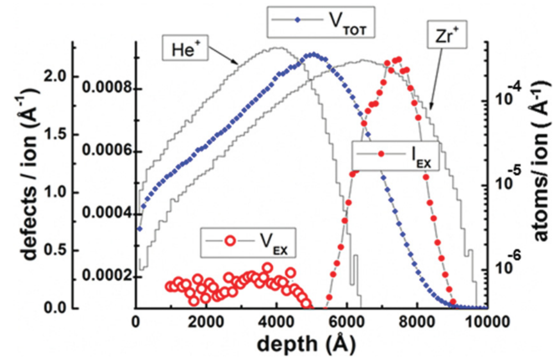

FIG. 1. (Color online) TRIM simulation of depth profiles for 2.5 MeV Zr^+ and 100 keV He^+ implantation into ZrO_2 under an incidence angle of 22.5° (right scale). The irradiation induced depth distributions of excess vacancies (V_{EX}) and excess interstitials (I_{EX}) generated by Zr^+ implantation (red circles, left scale) were calculated with the consideration of additional interstitials introduced by the implanted Zr atoms (+1 atoms). The total amount of displacements (V_{TOT}) is also shown (blue squares, leftmost scale).

reordering or diffusion process. The profiles presented by red circles take into account the implanted Zr atom (+1 atom), which is counted as an interstitial atom. The depth profile of the Zr^+ implantation induced V_{EX} extends from the surface to the depth of about 500 nm which matches well with the implanted 100 keV helium profile. The I_{EX} peak at about 720 nm is somewhat deeper. About 0.67 excess vacancies are generated per implanted Zr^+ ion.

B. Rutherford backscattering /channeling

Figure 2(a) presents RBS spectra of the virgin and irradiated YSZ samples. The random spectrum $R(x)$ taken from the virgin YSZ sample shows the Zr surface edge at channel 750 and the O edge near channel 300. The aligned spectrum of virgin YSZ taken in ⟨100⟩ channeling direction shows a much lower backscattering yield and is nearly identical with the aligned spectrum of the helium irradiated sample. This demonstrates the good crystal quality of the virgin sample $\chi_{min} \sim 7\%$, and indicates that the sensitivity of RBS is not high enough to detect the defects induced by helium irradiation with a fluence of 5×10^{15} cm^{-2}. However, the aligned backscattering yields of other irradiated samples are significantly higher. The damage profiles $D(x)$ of the samples irradiated by DB implantation and single Zr^+ implantation in Fig. 2(b) are calculated using the relation

$$D(x) = [A(x) - d(x)]/[R(x) - d(x)],$$

where $A(x)$, $R(x)$, and $d(x)$ are the aligned backscattering spectrum, the random backscattering spectrum, and the fitted dechanneling baseline, respectively. The line $d(x)$ represents the calculated backscattering yield at a certain depth x taking into account only the additional dechanneling of particles at lower depths due to the lattice defects located therein. Consequently, the dechanneling at a depth $x(i)$ corresponding to channel i can be calculated as $d[x(i)] = d[x(i-1)] + k\ A(i-1)/R(i-1)$. The factor k represents the ability of the defects to deflect the ions from the channeled direction and depends on the kind of defects as well as on the

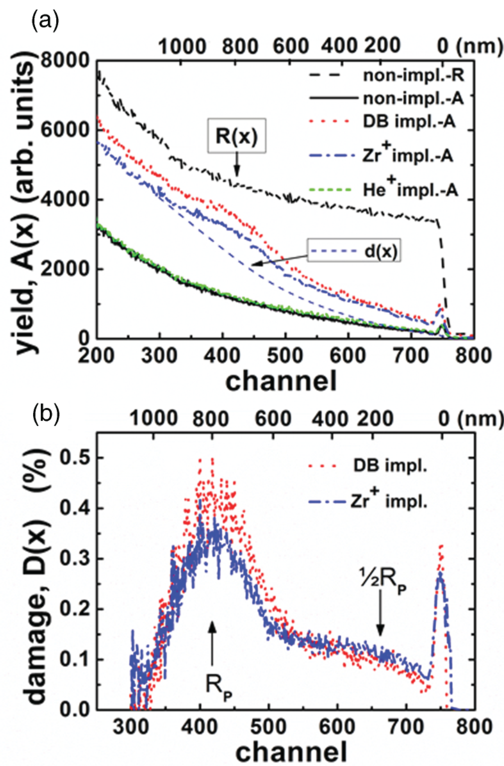

FIG. 2. (Color online) (a) RBS spectra of YSZ crystals recorded in random and ⟨100⟩-axial directions for irradiation by DB, Zr^+ implantation and He^+ implantation. $d(x)$ is the fitted dechanneling baseline indicated for the Zr^+ implantation. The upper scale indicates the depth position. (b) Damage profiles as generated by DB and Zr^+ implantation. The profiles are calculated from the corresponding RBS spectra shown in (a). Two damage peak positions are indicated by arrows termed as R_p and $\frac{1}{2}R_p$. They are related to the so called $\frac{1}{2}R_p$ effect. The sharp peak at channel 750 is due to backscattering from the sample surface.

beam parameters. k is calculated by considering that the dechanneling line $d(x)$ should fit the aligned spectrum $A(x)$ at greater depths, where no lattice defects are expected [see Fig. 2(a) at channels $i < 320$]. Except for the surface peak at channel 750 two damage peaks are detected at channels 420 and 675, which are indicated in Fig. 2(b) as R_p and $\frac{1}{2}R_p$, respectively. The $\frac{1}{2}R_p$ damage peak is closer to the surface at the depth range around 200 nm and is significantly smaller than the R_p peak at 800 nm.

C. High resolution x-ray diffraction

For the characterization of the structural properties HRXRD was applied with a very high sensitivity to lattice parameter changes. Reciprocal space maps were measured at the symmetric (002) and (004) reflections. From these scans the vertical strain profiles of the samples were calculated. The diffracted signal was simulated using a recursive dynamical algorithm implemented in the commercial program "RC_REF_Sim_Win."[27] It is assumed that the whole implanted region stays almost crystalline as supported by the nearly unchanged Debye-Waller factors for the virgin sample, the as-implanted one and after annealing. From these

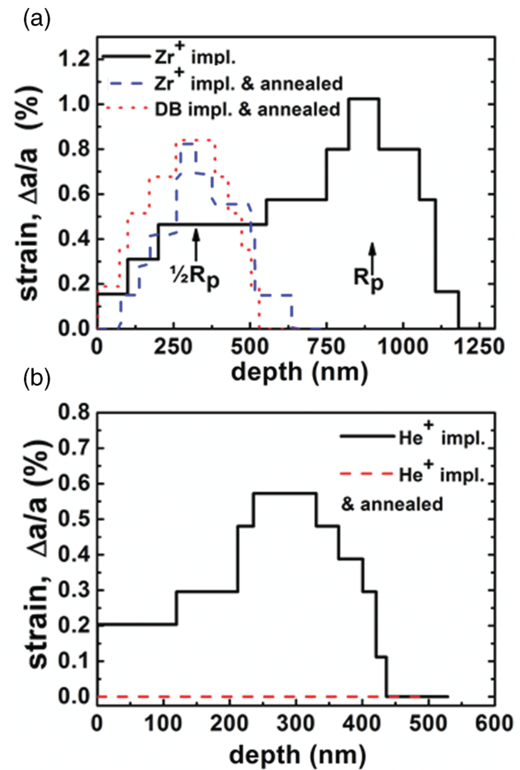

FIG. 3. (Color online) Strain depth profiles obtained from the high resolution x-ray scattered intensity distribution on YSZ crystals irradiated by (a) DB, Zr^+ implantation and (b) He^+ implantation. The annealed samples were thermally processed at 800 °C for 1 h. The peak position related to the $\frac{1}{2}R_p$ effect for open volume defect formation is marked by an arrow.

measurements an irradiation-induced uniaxial strain field can be easily deduced. The lattice constant of the implanted layer expands in direction normal to the sample surface. Annealing results in relaxation of the generated strain field, that is, the vertical lattice expansion, is completely (for He^+ implantation) or partially removed. Figure 3 shows vertical lattice strain profiles of the samples obtained from the HRXRD measurement. The strain profile in Fig. 3(a) for the Zr^+ implanted YSZ sample (black solid line) extends over the whole implanted depth range from the surface to 1100 nm. The main strain peak located at a depth of 850 nm shows a relatively high strain level with a deviation of about 1% of the lattice constant, while the shoulder of the strain profile with a strain level of about half the maximum value is located around 380 nm. The strain profile of the DB implanted sample has almost the same features as the Zr^+ implanted sample, and therefore it is not shown. After annealing at 800 °C for 1 h the strain peak at 850 nm in both samples, Zr^+ and DB implanted ones, completely disappears. In contrast, a new strain peak is formed at the depth range around 320 nm in the region of the shoulder of the nonannealed strain profile (blue dashed and red dotted lines). This depth position is indicated as $\frac{1}{2}R_p$, whereas the deeper strain peak is indicated as R_p. Strain in the as-implanted sample is due to uniaxial lattice expansion in direction of the surface normal. During annealing the lattice relaxes in the depth range of the R_p strain peak while lattice expansion is increased at the $\frac{1}{2}R_p$ region.

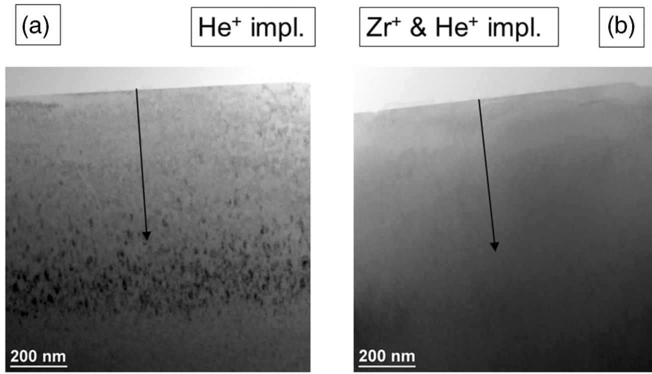

FIG. 4. Cross-sectional TEM images of a (a) He^+ implanted YSZ sample and a (b) DB (Zr^+ and He^+) implanted sample. In this case helium was implanted to 1×10^{16} cm^{-2} with an ion energy of 260 keV. The length of the arrows indicates the depth range from surface to 500 nm. Black dots are dislocation loops.

The strain profile of the He^+ implanted sample in Fig. 3(b) shows a similar depth distribution as the Zr^+ implanted sample. However, the strain value is reduced due to less fluence and damage generation by He^+ implantation, and the strain completely disappears after annealing.

D. Transmission electron microscopy

Figure 4 shows cross-sectional TEM images of He^+ ion and DB implanted YSZ specimen. These samples were implanted with a fluence of 1×10^{16} He cm^{-2} and an helium ion energy of 260 keV. The dark spots visible in Fig. 4(a) for He^+ implantation are dislocation loops. Their depth position corresponds to the calculated I_{EX} profile. No such defects are found in the DB implanted specimen. In this case [Fig. 4(b)] the sample seems to be perfectly recovered. A closer inspection of the $\frac{1}{2}R_p$ region of the specimens by HRTEM reveals a large number of helium bubbles only in the He^+ implanted sample which are demonstrated in Fig. 5 by over-focus and under-focus TEM images.

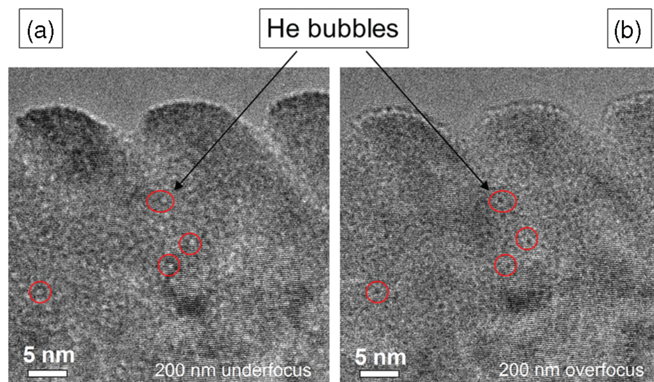

FIG. 5. (Color online) High resolution TEM images of the He^+ implanted YSZ sample [Fig. 4(a)] at the depth position of 300 nm. Circles mark small helium bubbles with diameters of about 1 nm shown in (a) under-focus and (b) over-focus.

E. Positron annihilation spectroscopy

Vacancies in the range of a mono-vacancy to vacancy clusters consisting of about 25 vacancies can be detected by means of PAS. Positrons have a higher possibility to be trapped and annihilated (under emission of two 511 keV photons) at open volume sites in materials, where the local electron density is lower due to the reduced atomic density. S (shape) and W (wing) are two major parameters of the Doppler broadened 511 keV line spectra in positron annihilation measurements. S is defined as the ratio of the amount of quanta in the central part of the annihilation peak (here 510.03–511.97 keV) to the quanta in the complete peak (498.5–523.5 keV). W is the corresponding ratio for the wing range of the annihilation line (513.76–516.06 keV plus 505.94–508.24 keV). The measured S and W parameters can give information about the nature and concentration of open volume defects as well as the atomic environment of the annihilation site. A high S parameter is due to annihilation of the positrons inside the open volume, whereas a high W parameter indicates annihilation with higher momentum electrons close to matrix atoms. Figure 6(a) shows the S parameter as a function of the positron energy and above the corresponding calculated depth scale. S profiles of Zr^+ and DB implanted samples exhibit the same features. That proves the simultaneous implantation of He^+ does not play a role for

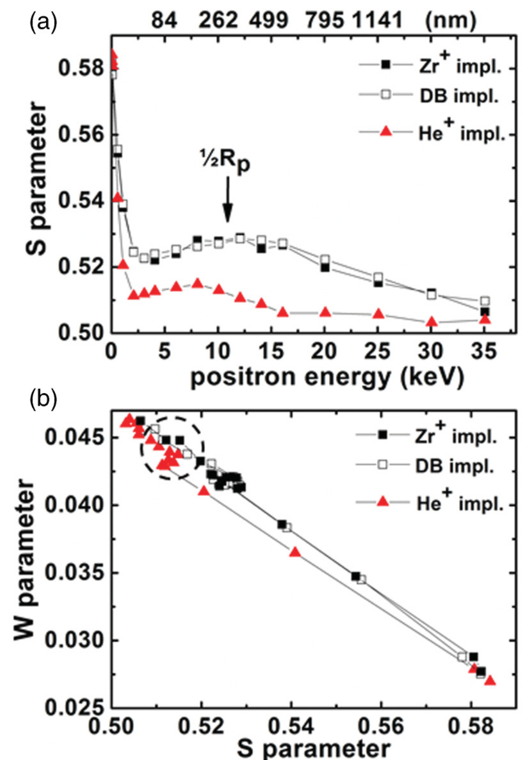

FIG. 6. (Color online) (a) S parameter data as a function of incident positron energy for YSZ crystals irradiated by DB, single Zr^+ and single He^+ implantation. The depth corresponding to the positron energy is plotted by the upper scale. An arrow marks the peak position related to the $\frac{1}{2}R_p$ effect for open volume defect formation. (b) W-S plot of YSZ crystals irradiated by DB, Zr^+ and He^+ implantation. The deviation of the W-S curve from a straight line is marked by a dashed circle.

generation of open volume defects. The peak position of the S profiles for Zr^+ and DB implantation is at 12 keV and for He^+ implantation with 100 keV at 8 keV. This depth range is clearly in approximate agreement with the $\frac{1}{2}R_p$ damage peaks observed by RBS [Fig. 2(b)] and XRD [Fig. 3(a)]. For positron energies of 35 keV all S parameters profiles converge to the bulk value of YSZ.

In order to compare the type of the open volume defects the measured data are shown by the W-S plot in Fig. 6(b). Data points on the right side of Fig. 6(b) represent positron annihilation in open volume (high S parameter) and those on the left side represent positron annihilation closer to atoms of the environment (high W parameter). All data points are located on a straight line if there is only one type of open volume defects, which only differ in their concentration as a function of the depth position. This is fulfilled for Zr^+ and DB implantation. However, the defects generated by He^+ implantation deviate from this line especially for annihilation close to the environmental atoms (high W parameter). There is also a sharp kink in the W-S line for He^+ implantation. This can be explained by two types of defects, empty vacancy clusters and others with helium atoms trapped inside.

The above results are confirmed by coincidence Doppler broadening spectroscopy, an analysis method especially sensitive to the environment of the positron annihilation site. The measurement was performed for the reference sample with higher helium concentration. Figure 7 shows the count ratio of DB irradiated and single Zr^+ ion beam irradiated YSZ samples to the nonirradiated bulk. p_L is the momentum of the electron that annihilates with the positron. A low momentum (free-electron) is ascribed to an annihilation site in open volume, whereas a high momentum (valence electron) indicates an annihilation site closer to an environmental atom. The agreement between the curves for Zr^+ (no He^+ implanted) and DB (Zr^+ and He^+ implanted) proves the absence of helium in open volume defects of the DB implanted sample.

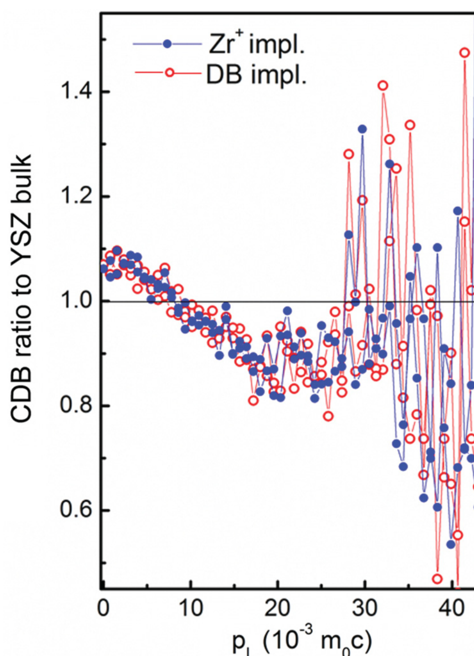

FIG. 7. (Color online) Coincidence Doppler broadening ratio curves of DB irradiated YSZ (2.5 MeV Zr^+ and 260 keV He^+ ions) and of single Zr^+ ion irradiated YSZ. The positron energy was 12 keV.

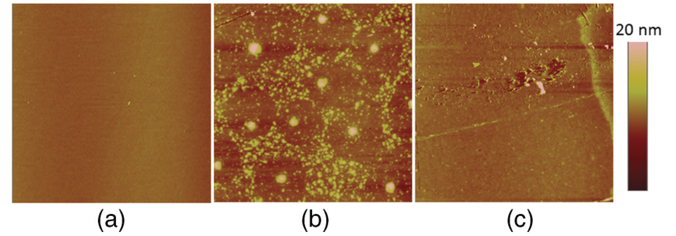

FIG. 8. (Color online) AFM images: (a) virgin YSZ surface, (b) single He^+ implanted YSZ surface, and (c) DB (Zr^+ and He^+) implanted YSZ surface. The scanned area is 10 μm × 10 μm. The height scale bar (right) is 20 nm.

F. Atomic force microscopy

The atomic force microscopy (AFM) investigation of the YSZ surfaces confirms the results of the PAS analysis. Comparing the virgin YSZ sample surface [Fig. 8(a)] the single He^+ ion implanted sample shows the appearance of many self-ordered nanohills on the surface [Fig. 8(b)]. These features indicate the formation of helium bubbles which coalesce and result in the local lift-off of the surface layer. This finding as well as the XRD profiles in Fig. 3(b) are in full agreement with recent results of Velisa *et al.*[16] who reported the deleterious effect of a high fluence single He^+ ion beam implantation. However, for the simultaneous implantation with Zr^+ ions [Fig. 8(c)] the surface remains smooth.

IV. DISCUSSION

A. The $\frac{1}{2}R_p$ effect

The different relative sensitivity of the analysis methods to interstitial-type and vacancy-type defects has to be taken into account in order to consider if the $\frac{1}{2}R_p$ effect can be proven for ion implantation into YSZ. RBS/channeling analysis is clearly sensitive to interstitials. Consequently the damage profiles in Fig. 2(b) show a significant R_p damage peak at the depth of 800 nm which is in good agreement with the I_{EX} profile calculated by TRIM. Note that the TRIM simulation does not account for ion channeling, a process which always occurs for implantation into crystalline targets and may result in a slightly deeper damage profile as compared to the simulation. There is also damage indicated in the $\frac{1}{2}R_p$ region in Fig. 2(b). This damage appears much weaker as it results from the strain field around the vacancy clusters. RBS alone cannot determine the type of defects at $\frac{1}{2}R_p$ and R_p (either vacancies or interstitials). However, the different annealing behavior of defects at $\frac{1}{2}R_p$ and at R_p seen by XRD [Fig. 3(a)] and the missing dislocation loops in the $\frac{1}{2}R_p$ region in TEM images (Fig. 4) clearly indicate the vacancy character of the defects at $\frac{1}{2}R_p$. The strain profile measured by XRD is very similar to the damage profile determined by RBS with exception of the relative damage level at $\frac{1}{2}R_p$ which is higher for the XRD analysis. During annealing the lattice completely relaxes at R_p due to recrystallization

TABLE I. Summary of the damage peak positions from different characterization methods obtained for single Zr^+ ion and DB (2.5 MeV Zr^+ and 100 keV He^+) ion implanted zirconia.

Methods	Damage peak I (excess vacancy related)	Damage peak II (excess interstitial related)
TRIM	~350 nm	~740 nm
HR-XRD	~375 nm (as-implanted)	~870 nm (as-implanted)
	350 nm (annealed)	–
RBS	~220 nm	~800 nm
PAS	~380 nm	–

and the incorporation of the +1 atoms on lattice sites. At the $\frac{1}{2}R_p$ region vacancy clusters grow as indicated by the strain peak appearing in the depth range between surface and 500 nm. The formation of vacancies or small vacancy clusters in the $\frac{1}{2}R_p$ region during implantation is demonstrated by PAS results shown in Fig. 6(a). PAS is sensitive only to open volume defects and allows us to detect mono-vacancies and small vacancy clusters. However, the depth distribution of the positrons in YSZ becomes very broad with increasing positron energy. Therefore, the measured profile is smeared out. This explains the slow decrease of the S parameter profile with increasing positron energy.

Table I summarizes the peak positions of the damage profiles observed from the different methods. It is clearly demonstrated that there are two damage regions in Zr^+ and DB implanted YSZ samples. This is in agreement with the TRIM simulation. The damage peak I in the depth range until 500 nm is ascribed to V_{EX} defects, whereas the damage peak II at 800 nm is related to I_{EX} defects. The occurrence of the $\frac{1}{2}R_p$ effect in YSZ is reliable, proven as its magnitude is reduced in this experiment because the implantation direction is inclined under 22.5°.[24]

B. Dual beam implantation and helium release

According to Saudé *et al.*[22] one expects that the trapping and accumulation of He atoms would stabilize and enlarge the vacancy clusters generated in the $\frac{1}{2}R_p$ region by Zr^+ ions. Implantation induced vacancy clusters are clearly detected by PAS. However, all the analysis methods show no significant difference between single beam Zr^+ implantation and the DB (Zr^+ and He^+) implantation. Obviously the damage is exclusively induced by the Zr^+ ions as the contribution of the He^+ ions is negligible. For single beam He^+ implantation the W-S plot in Fig 6(b) indicates a different type of open volume defects which was attributed to the presence of helium in the vacancy clusters. Such defects are not seen in DB implanted YSZ. The vacancy defects induced by single beam Zr^+ implantation are consistent with the DB defects and of course helium-free. Consequently, helium is released at room temperature from the vacancy defects by DB implantation.

First-principles total energy calculations based on the density functional theory (DFT) were performed in the generalized gradient approximation using the functional of Perdew, Burke, and Ernzerhof[28] for the exchange correlation potential. This calculation can estimate the microscopic dissolution behaviors of helium[29] in ZrO_2. The results show that the solution energy of helium is 1.43 eV at the most stable interstitial lattice site. It is the position with the lowest electron density.[30] Apparently a structure with a vacancy will further decrease the electron density. Energy minimization finds the most stable site for He atoms in a Zr vacancy at the vacancy center. There, the solution energy is 0.92 eV lower than at the interstitial site, and thus the trapping energy of a He atom at the vacancy is −0.92 eV. This result is confirmed by first-principles calculations of Zhang *et al.*[31] who stated the Zr vacancy (rather than the O vacancy) to be the preferential trapping center in ZrO_2 for helium, whereas it is almost insoluble in the undisturbed lattice. Therefore, the vacancy-assisted diffusion of helium in ZrO_2 is more likely than the interstitial diffusion.

This finding matches well to experimental investigations reporting the fluence dependent thermal release of helium from zirconia with an activation enthalpy of 2 eV.[32] Dissociation from vacancies starts at temperatures around 400 °C[32] and the complete degassing from bubbles in YSZ is reached at temperatures above 800 °C.[33] Above all the out-diffusion of implanted hydrogen from YSZ was observed during the ensuing ion beam analysis at room temperature.[34] Considering that one incoming Zr^+ ion creates about 5870 Zr vacancies along its path, there is a high Zr-vacancy concentration under our DB implantation conditions to trap helium atoms. Otherwise, the average energy transferred to each Zr atom far exceeds the energy necessary to release the helium atom from its trap. For that reason a Zr-vacancy assisted trapping/detrapping diffusion mechanism is assumed to be active for out-diffusion of helium from YSZ under DB implantation conditions.

V. SUMMARY

The radiation damage in YSZ was investigated using single beam (He^+ or Zr^+) and simultaneous dual beam (He^+ and Zr^+) implantations. The amount and type of the damage formed in dual beam implanted YSZ are found to be the same as for single beam Zr^+ implanted YSZ. Damage generation by He^+ ions can be neglected in comparison to damage generation by Zr^+ ions. No helium related effect is detected regarding the defect formation in dual beam implanted YSZ. The materials morphology stays almost unmodified. The mobilization and out-diffusion of helium at room temperature from the implanted region is due to the simultaneous Zr^+ implantation. In contrast, helium trapping in vacancy clusters and helium bubble formation was found for single He^+ ion beam implanted YSZ. In this case the coalescence of helium bubbles results in a local swelling and lift-off at the surface.

Helium is trapped in YSZ preferentially by Zr vacancies with an energy of −0.92 eV. Out-diffusion under irradiation proceeds by a vacancy driven trapping/detrapping mechanism. The release of helium from vacancy defects is a contributing factor that causes the excellent characteristics of YSZ under irradiation.

Furthermore, the spatial separation of implantation induced vacancies and interstitials was demonstrated in ion irradiated YSZ. The distribution of the vacancy and interstitial related damage is in agreement with TRIM simulations. This process corresponds to the so called $\frac{1}{2}R_p$ effect and has to be carefully

considered in the evaluation of implantation based experiments simulating isotropic irradiation effects such as the α decay in materials. The accumulation of vacancy defects in a layer at $\frac{1}{2}R_p$ and the trapping of helium are in particular critical for void or cavity formation and may lead to embrittlement and blistering in a worst case.

ACKNOWLEDGMENTS

The authors are very thankful to the anonymous reviewers of our manuscript as they gave us the motivation to carefully revise and improve the manuscript. The authors also thank the contribution of the technicians in the ion beam center of HZDR for operation of the irradiation facilities.

[*]Corresponding author: X.ou@hzdr.de

[1]S. J. Zinkle and J. T. Busby, Mater. Today **12**, 12 (2009).
[2]A. Meldrum, S. J. Zinkle, L. A. Boatner, and R. C. Ewing, Nature (London) **395**, 56 (1998).
[3]W. J. Weber, R. C. Ewing, C. R. A. Catlow, T. D. de la Rubia, L. W. Hobbs, C. Kinoshita, H. Matzke, A. T. Motta, M. Nastasi, E. K. H. Salje, E. R. Vance, and S. J. Zinkle, J. Mater. Res. **13**, 1434 (1998).
[4]W. L. Gong, W. Lutze, and R. C. Ewing, J. Nucl. Mater. **277**, 239 (2000).
[5]C. Degueldre, U. Kasemeyer, F. Botta, and G. Ledergerber, Mater. Res. Soc. Symp. Proc. **412**, 15 (1996).
[6]S. Moll, L. Thomé, L. Vincent, F. Garrido, G. Sattonnay, T. Thomé, J. Jagielski, and J. M. Costantini, J. Appl. Phys. **105**, 023512 (2009).
[7]L. Thomé and F. Garrido, Vaccum **63**, 619 (2001).
[8]A. Debelle, A. Declémy, L. Vincent, F. Garrido, and L. Thomé, J. Nucl. Mater. **396**, 240 (2010).
[9]C. Jiang, X. Y. Liu, and K. E. Sickafus, Phys. Rev. B **83** 052103 (2011).
[10]A. Meldrum, S. J. Zinkle, L. A. Boatner, and R. C. Ewing, Phys. Rev. B **59**, 3981 (1999).
[11]N. Yu, K. E. Sickafus, P. Kodali, and M. Nastasi, J. Nucl. Mater. **244**, 266 (1997).
[12]S. Zhou, A. Shalimov, Y. Wang, and K. Potzger, J. Nucl. Mater. **416**, 358 (2011).
[13]Y. Zhang, W. Jiang, C. M. Wang, F. Namavar, P. D. Edmondson, Z. Zhu, F. Gao, J. Lian, and W. J. Weber, Phys. Rev. B **82**, 184105 (2010).
[14]P. D. Edmondson, W. J. Weber, F. Namavar, and Y. Zhang, Scr. Mater. **65**, 675 (2011).
[15]L. Thomé, J. Fradin, J. Jagielski, A. Gentils, S. E. Enescu, and F. Garrido, Eur. Phys. J.: Appl. Phys. **24**, 37 (2003).
[16]G. Velisa, A. Debelle, L. Vincent, L. Thomé, A. Declémy, and D. Pantelica, J. Nucl. Mater. **402**, 87 (2010).
[17]T. Yang, X. Huang, Y. Gao, C. Wang, Y. Zhang, J. Xue, S. Yan, and Y. Wang, J. Nucl. Mater. **420**, 430 (2012).
[18]A. Peeva, R. Kögler, W. Skorupa, J. S. Christensen, and A. Yu. Kuznetsov, J. Appl. Phys. **95**, 4378 (2004).
[19]X. Ou, R. Kögler, A. Mücklich, W. Skorupa, W. Möller, X. Wang, and L. Vines, Appl. Phys. Lett. **94**, 011903 (2009).
[20]R. Kögler, A. Peeva, P. Werner, W. Skorupa, and U. Gösele, Nucl. Instrum. Methods B **175**, 340 (2001).
[21]X. Ou, R. Kögler, A. Mücklich, W. Skorupa, W. Möller, X. Wang, J. W. Gerlach, and B. Rauschenbach, Appl. Phys. Lett. **93**, 161907 (2008).
[22]S. Saudé, R. I. Grynszpan, W. Anwand, G. Brauer, J. J. Grob, and Y. Le Gall, Nucl. Instrum. Methods B **216**, 156 (2004).
[23]H. Trinkaus and B. N. Singh, J. Nucl. Mater. **323**, 229 (2003).
[24]R. Kaschny, R. Kögler, H. Tyrrof, W. Bürger, F. Eichhorn, A. Mücklich, C. Serre, and W. Skorupa, Nucl. Instrum. Methods A **551**, 200 (2005).
[25]J. P. Biersack and L. G. Haggmark, Nucl. Instrum. Methods B **174**, 257 (1980).
[26]R. Kögler, A. Peeva, J. R. Kaschny, W. Skorupa, and H. Hutter, Nucl. Instrum. Methods B **186**, 298 (2002).
[27]P. Zaumseil, Phys. Status Solidi A **165**, 195 (1998).
[28]J. P. Perdew, K. Burke, and M. Ernzerhof, Phys. Rev. Lett. **77**, 3865 (1996).
[29]Y. Zhang, W. Feng, Y. L. Liu, G. H. Lu, and T. Wang, Nucl. Instrum. Methods B **216**, 3200 (2009).
[30]M. J. Puska and R. M. Nieminen, Phys. Rev. B **43**, 12221 (1991).
[31]P. Zhang, Y. Lu, C.-H. He, and P. Zhang, J. Nucl. Mater. **418**, 143 (2011).
[32]P. M. G. Damen, A. van Veen, F. Labohm, H. Schut, and M. A. van Huis, J. Nucl. Mater. **319**, 65 (2003).
[33]J.-M. Costatini, J.-J. Grob, J. Haussy, P. Trocellier, and Ph. Trouslard, J. Nucl. Mater. **321**, 281 (2003).
[34]Y. Zhang and W. J. Weber (private communication).